Hindawi Publishing Corporation
International Journal of Photoenergy
Volume 2012, Article ID 368750, 10 pages
doi:10.1155/2012/368750

Research Article

Synthesis, Characterization, and Photocatalysis of Fe-Doped TiO_2: A Combined Experimental and Theoretical Study

Liping Wen,[1] Baoshun Liu,[1,2] Xiujian Zhao,[1] Kazuya Nakata,[2,3] Taketoshi Murakami,[2] and Akira Fujishima[2,3]

[1] *State Key Laboratory of Silicate Materials for Architectures, Wuhan University of Technology, Wuhan City, Hubei Province 430070, China*
[2] *Photocatalyst Group, Kanagawa Academy of Science and Technology, KSP East 412, 3-2-1 Sakado, Takatsu-ku, Kawasaki, Kanagawa 213-0012, Japan*
[3] *Division of Photocatalyst for Energy and Environment, Research Institute for Science and Technology, Tokyo University of Science, 1-3 Kagurazaka, Shinjuku-ku, Tokyo 162-8601, Japan*

Correspondence should be addressed to Baoshun Liu, liubaoshun@126.com and Kazuya Nakata, pg-nakata@newkast.or.jp

Received 6 January 2012; Revised 25 February 2012; Accepted 27 February 2012

Academic Editor: Baibiao Huang

Fe-doped TiO_2 was prepared by hydrothermal treating Ti peroxide sol with different amount of iron nitrate. Fe ions can enter TiO_2 lattice by substituting Ti^{4+} ions, which significantly affect the crystallinity and morphology of TiO_2 nanoparticles. Fe doping also influences the UV-Vis absorption and photoluminescence of TiO_2, due to the change of electronic structure. It is shown that Fe ions are more easily doped on TiO_2 surface than in bulk. The theoretical computation based on the density functional theory (DFT) shows that the Fe ions in TiO_2 bulk are localized and mainly act as the recombination centers of photoinduced electrons and holes. Some results support that the Fe^{3+} ions on surface can form intermediate interfacial transfer pathway for electrons and holes, which is beneficial for increasing the photocatalytic activity of TiO_2. The photocatalytic activity first increases and then decreases as the Fe concentration increases, which is coaffected by the bulk-doped and surface-doped Fe ions.

1. Introduction

Since the publishing of photocatalytic water splitting [1], photocatalysis has drawn much attention in the world for many years [2–4]. Compared with other photocatalysts, TiO_2 is extensively studied because of low-cost, non-toxicity, and high chemical-stability. Generally, pure TiO_2 suffers from problems of large band gap (E_g) [5, 6] and low quantum yield. Doping is proved to be effective to narrow E_g and increases photocatalytic activity [7–14]. Transition-metal-doped TiO_2 have been widely studied due to their d electronic configuration [15–18]. Fe is the most studied because it has the radium identical to Ti^{4+} and the half-filled d electronic configuration [19–21]. It was reported that the photocatalytic activity of Fe-doped titanate nanotubes is 2 times higher than P25 under visible light illumination [19], and the Fe-doped Q (quantum)-TiO_2 particles can remove chloroform under UV light illumination due to the trapping of photoinduced electrons and holes [20].

It is always reported that the photocatalytic activity under UV light illumination will firstly increase and then decrease with the increase of doped Fe concentration [17, 19, 20]. It is considered that the Fe ions can trap holes or electrons for low-level doping, while they will change to recombination centers for high-level doping [17, 19, 22]. However, the physical reason that the doped Fe^{3+} ions mainly act as recombination centers is not well known. Although tunneling recombination is said to become significant for high doping level, no experimental proofs can support this conclusion. The research 20 devoted to studying the photocatalytic mechanism of transition-metal-doped Q-TiO_2 particles of 3-4 nm. In this case, Fe ions are mainly on surface due to the small particle size, which can form effective pathways for charge interfacial transfer. For example, Wang et al. reported that the Fe^{3+} ions can combine with the hydroxyl groups on TiO_2 nanoparticle surface and form $(OH)Fe^{3+}$ complexes, which is a good way for electron

transfer [23]. Other ions, such as Cu^{2+} ions, on TiO_2 surface can also promote the electron transfer, and the mechanism of multielectron transfer is suggested [24, 25]. Compared with the Q-particles, the specific surface area decreases for large particles (>15 nm), and it is possible for the Fe ions to enter TiO_2 bulk beside surface. Since the carrier exciton Bohr radius in TiO_2 is ca. 2 nm [20], the holes or electrons trapped at Fe ions in bulk are difficult to migrate to surface before going to recombination. It is also reported that the optimal Fe-doped concentration is dependent on the particle size [26], and the increase of particle sizes will result in the decrease of optimal concentration, which may be due to that more Fe ions that enter the bulk for larger particles can increase the recombination of electrons and holes. It predicts that the Fe ions on surface may increase the photocatalytic activity, while the Fe ions in bulk will have negative effect.

However, the different effect of bulk dopant and surface dopant on photocatalysis is not systematically investigated. In this work, we aim to discuss the different functions of Fe ions on surface and in bulk during photocatalysis under UV light illumination. It is found that the surface doping is dominant for low-level doping, and more Fe ions will enter TiO_2 bulk with the increase of doping concentration. The ab initio computation based on density functional theory (DFT) shows that the Fe ions in TiO_2 bulk are localized, indicating that they mainly act as the recombination centers of electrons and holes. It is suggested that the role change of Fe ions from trapping to recombination centers as the doped Fe concentration increases is related to the transformation from surface to bulk doping, and this transformation explains the photocatalytic behavior of Fe-doped TiO_2 observed by us and other researchers.

2. Experimental

2.1. Sample Preparation. The TiO_2 samples were synthesized using hydrothermal method. $TiCl_4$ and $Fe(NO_3)_3$ were used as the precursors of TiO_2 and Fe ions. 4.0 mL $TiCl_4$ was added to 400 mL ice distilled water under vigorous stirring, and then, the resulted solution was stirred for 24 h at room temperature. Subsequently, ammonia aqueous solution (1 : 9) was added to adjust the solution pH to ca. 7 to get $Ti(OH)_4$ precipitation. The precipitation was filtered and cleaned using distilled water for many times. Afterwards, the $Ti(OH)_4$ precipitation was dispersed in ice-distilled water. 30% H_2O_2 was dropped until it became yellow and transparent. A designed amounts of $Fe(NO_3)_3$ were added under stirring, and then, the solutions were heated in enclosed autoclave for 12 h at 160°C to get Fe-doped TiO_2 hydrosols. A series of Fe-doped TiO_2 samples were prepared with the Fe: Ti molar ratio being 0, 0.1, 0.3, 0.5, 0.8, 1.0, 2.0, and 5.0 at. %, respectively. Finally, the hydrosols were dried at 40°C to obtain the powders.

2.2. Characterization. The X-ray diffraction (XRD) patterns were collected in the range of 20–80°(2θ) with a HZG4-PC diffractometer using Cukα radiation with an accelerating voltage of 40 kV and current of 40 mA ($\lambda_x = 1.5406$ A). The surface composition and element chemical states of Fe-doped samples were characterized by an X-ray photoelectron spectroscopy (XPS) in an ESCA system with monochromatic Mg kα source and a charge neutralizer. The particle morphologies ware observed with a JEM-2001 transmittance electron microscope (TEM) at an acceleration voltage of 200 kV. Diffused reflectance spectra were recorded on a Shimadzu UV2550-UV spectrophotometer equipped with an integrating sphere assembly in the range of 190–700 nm, with $BaSO_4$ used as the reference. The photoluminescence (PL) spectra were measured at room temperature with Shimadzu RF-5301 fluorospectrophotometer by using 320 nm line of Xe lamp as excitation source. The energy-dispersive X-ray (EDX) equipped on the JSM-7500F field emission scanning electron microscope was used to detect the real element concentrations in the Fe-doped TiO_2 samples.

2.3. Computational Detail. The computational calculation has been performed within DFT plane wave pseudo potential method. The general gradient approximation (GGA) with the Perdew-Burke-Ernzerhof (PBE) functional and ultra-soft pseudopotentials was used to describe the exchange-correlation effects and electron ion interactions. The kinetic energetic cutoffs of 24 and 288 Ry for the smooth part of electronic wave functions and augmented electron density were used. Quantum-ESPRESSO code, Pwscf package [27], was used to perform ab initio quantum calculation. Monkhorst-Pack (M-P) k-space sampling was adopted for geometry optimization and density of the electronic states (DOS) calculation. The convergence threshold for the self-consistency energy calculation was set to 10^{-8} Ry, and all atomic relaxations were carried out until all components of the residual forces were less than 10^{-3} Ry/Bohr. A $3 \times 3 \times 1$ supercell (i.e., 108 atoms of TiO_2 anatase matrix) with two adjacent Fe ions and an oxygen vacancy between them was employed to simulate Fe-doped reduced anatase TiO_2. A $2 \times 2 \times 1$ anatase supercell with one Fe ion substituting one titanium ion models the Fe-doped TiO_2 without oxygen vacancy. A $2 \times 2 \times 1$ supercell with one oxygen vacancy was constructed to model the reduced anatase. In addition, pure TiO_2 unit cell was also calculated for comparison. $4 \times 4 \times 3$ and $2 \times 2 \times 3$ M-P grids for 48 supercell and 108 atom supercell were used for geometry optimization, and $8 \times 8 \times 6$ and $4 \times 4 \times 6$ M-P grids for 48 supercell and 108 atom supercell were used for DOS calculation. For the unit cell calculation (pure TiO_2), a $6 \times 6 \times 3$ and $12 \times 12 \times 6$ M-P grids were used for geometry optimization and density of states (DOSs) calculation.

2.4. Photocatalytic Activity Evaluation. The photocatalytic activities of the Fe-doped TiO_2 samples under UV were evaluated on the basis of the degradation rate of methyl orange (MO) in a 100×20 self-designed quartz reactor containing 0.3 g of catalyst and 30 mL of 10 mg/L MO aqueous solution. Prior to photocatalytic reactions, the suspension was allowed to reach adsorption equilibrium by stirring in dark about 60 min. The irradiation was performed with a 365 nm 1300 μWcm^{-2}.

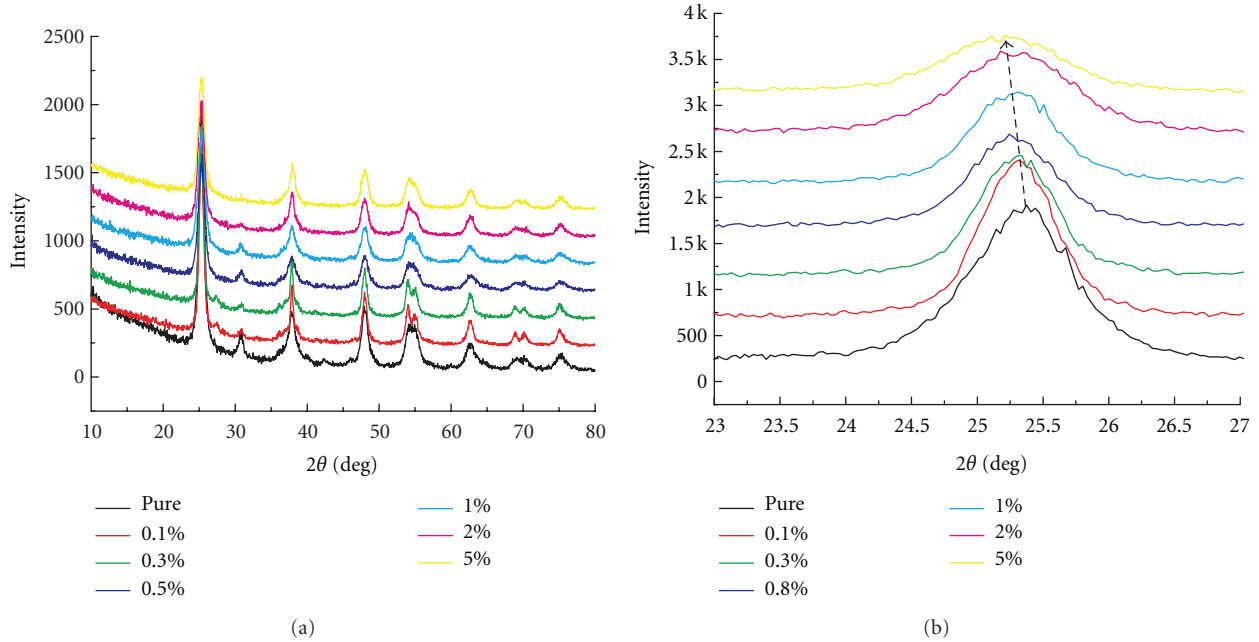

FIGURE 1: (A) The XRD patterns of the Fe-doped TiO_2 samples and (B) the magnified XRD (101) peak.

UV florescent lamp. In addition, the blank experiment without using UV illumination and TiO_2 photocatalyst was also conducted for comparison. Generally, the photocatalytic degradation follows a Langmuir-Hinshelwood (LH) mechanism for the low concentration [28, 29], and the reaction rate equation can be expressed as $\ln(C_0/C) = kt$, where C_0 and C are the initial concentration and reaction concentration, respectively.

3. Results and Discussion

3.1. Characterization. Figure 1(a) shows the XRD patterns of the Fe-doped TiO_2 samples. All of the as-prepared samples are mainly composed of anatase TiO_2. There is a little brookite, and its content becomes less and less with the increase of Fe concentration, indicating that Fe doping can restrain the brookite formation to some extent. The average anatase crystallite sizes decrease with the increase of Fe concentration because the doping restrains the grain growth [30, 31]. It can be seen from Figure 1(b) that the anatase (101) peak shifts to low 2θ direction as the Fe concentration increases, which indicates the (101) plane spacing becomes larger and larger when more and more Fe ions are doped. Because the radius of Fe^{3+} is a little smaller than that of Ti^{4+}, the widening of (101) plane spacing indicates that it is possible for some Fe^{3+} ions to enter the interstitial voids of TiO_2 lattice.

Figure 2 shows the TEM photos of pure (A-1), 2.0 at. % (B-1), and 5.0 at. % Fe-doped TiO_2 (C-1), with A-2, B-2, C-2 being their high-resolved photos. The pure sample is mainly composed of needles, sheets, and sticks. The TEM photos clearly show that the nanoparticles become smaller and smaller as the doped Fe content increases, which is in accordance with the XRD analysis. This is easy to be understood because doping foreign ions in TiO_2 lattice can actually prohibit the crystal growth. In addition, it can also be seen that the TiO_2 nanoparticles change to leaf-like morphology after Fe doping, indicating that Fe doping may also affect the particle growth. As shown in Figure 2, some white arrows are labeled to show the [001] crystal direction of anatase nanoparticles. The nanoneedles and sticks of the pure TiO_2 are long in [001] direction. After doping Fe, the length of [001] becomes shorter and shorter as the Fe-doped content increases. This result indicates that Fe doping may prohibit the nanoparticle growth in [001] direction.

Figure 3 shows the O1s, Ti2p, and Fe2p core spectra of the pure and Fe-doped samples (2.0 and 5.0 at. %). Ti2p peaks contain Ti2p1/2 and Ti2p3/2 subpeaks due to the spin-orbital coupling effect [32, 33]. The Fe doping almost has no effect on the Ti2p peak, indicating that Fe doping does not change the coordination and chemical state of Ti^{4+} ions. Compared with the symmetrical O1s peak of pure TiO_2 sample, a new broad peak at ca. 531.5 eV after Fe doping shows the absorption of hydroxyl groups on TiO_2 surface, which may indicate the formation of Fe^{3+}(OH) groups. It is reported that the Ti2p peak of N-doped TiO_2 shifts to low binding energy (BE) due to the bond weakening between nitrogen and titanium, implying that the nitrogen enters TiO_2 matrix by replacing oxygen ions [34]. In present research, the shifting of O1s peaks to high BE shows that the Fe doping changes the chemical coordination of oxygen. In addition, the Fe2p spectra show a positive shift as compared to those in Fe_2O_3, probably indicative of more positively charged surface Fe^{3+} [22]. The slight enhancement of Fe2p BE is due to the Fe^{3+} diffusion into TiO_2 lattice and the formation of Fe–O–Ti bond.

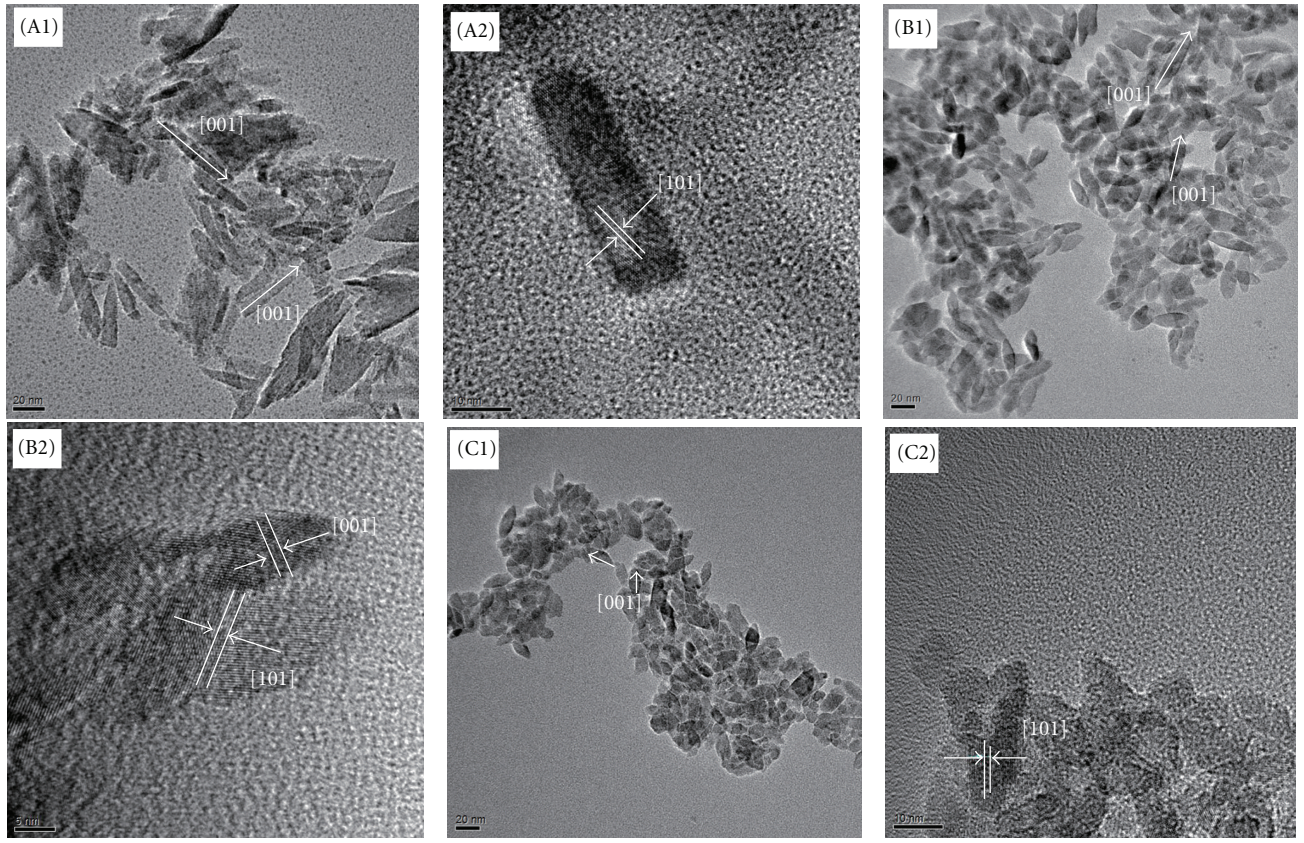

Figure 2: The TEM photos of pure TiO_2 (A) and the Fe-doped TiO_2 samples (2.0% (B) and 5.0% (C)).

The EDX area scanning technique was used to detect the average Fe on surface and in bulk. The 2.0 at. % and 5.0 at. % Fe-doped TiO_2 samples contain ca. 1.9 and ca. 4.9 at. % Fe ions. It can be seen that the Fe concentrations are very close to the designed values. The Fe content on surface checked using XPS is 8.2 at. % and 14.1 at. %, respectively. Therefore, it can be seen that the Fe ions are not uniformly distributed in but enrich on TiO_2 surface, in agreement with the study [35]. Since XPS is a detecting technique of surface chemical information of one and two atomic layers, it can be known that the Fe ions are enriched on TiO_2 surface. The ratio between the surface Fe concentrations and the designed values is ca. 4.31 and 2.82 for the 2.0 at. % and 5.0 at. % samples. Therefore, the surface doping becomes difficult gradually with the increase of doping concentration, which will make more Fe ions enter TiO_2 bulk.

Figure 4 shows the DRS spectra of the Fe-doped TiO_2 samples. The onset of the absorption edge for pure TiO_2 is at ca. 390 nm [36]. Those spectra show an obvious red shift after Fe doping, which is induced by the electron transition from Fe3d orbitals to TiO_2 conduction band (CB). The absorption peak at 480 nm is from the $d \rightarrow d$ transition ($T_{2g} \rightarrow A_{2g}$) [37], and it becomes clearer and clearer with the increase of Fe concentration. Figure 5 shows the normalized PL spectra of Fe-doped TiO_2 samples. The peak at 3.43 eV is from the CB → valence band (VB) recombination [38], and its density decreases gradually with the increase of Fe concentration due to the increase of non-irradiative recombination. The electrons and holes trapped on surface contribute to the PL band from 3.0 to 3.2 eV [39]. This band intensity decreases with the increases of Fe concentration, which shows that that Fe doping has a significant effect on surface electronic structure. Since the PL signal is from the recombination, lower PL intensity may indicate lower recombination [40, 41], which indicates that the surface Fe ions may increase the probability of interfacial transfer of photoinduced electrons and holes. The PL peaks within 2.6 and 2.75 eV are suggested to be from the indirect recombination via bulk defects [42]. The PL shoulders from 2.2 to 2.45 eV are from the deactivation of the photoinduced electrons in $[TiO_6]$ groups on TiO_2 surface [39], which also show that the Fe doping has little effect on the Ti–O chemical environment, in agreement with the XPS result.

3.2. Electronic Structure Investigation. Based on the experiments, DFT computations were performed. The projected density of states (PDOSs) is shown in Figure 6. It can be seen that the VB and CB of TiO_2 are mainly composed of O2p orbitals and Ti3d orbitals, respectively [42, 43]. For pure TiO_2 (Figure 6(a)), the Fermi level (E_F) locates in the middle of the forbidden band, indicating that VB is full filled, while CB is empty. The E_g of pure TiO_2 is ca. 1.9 eV, which is underestimated due to the well-known shortcoming of

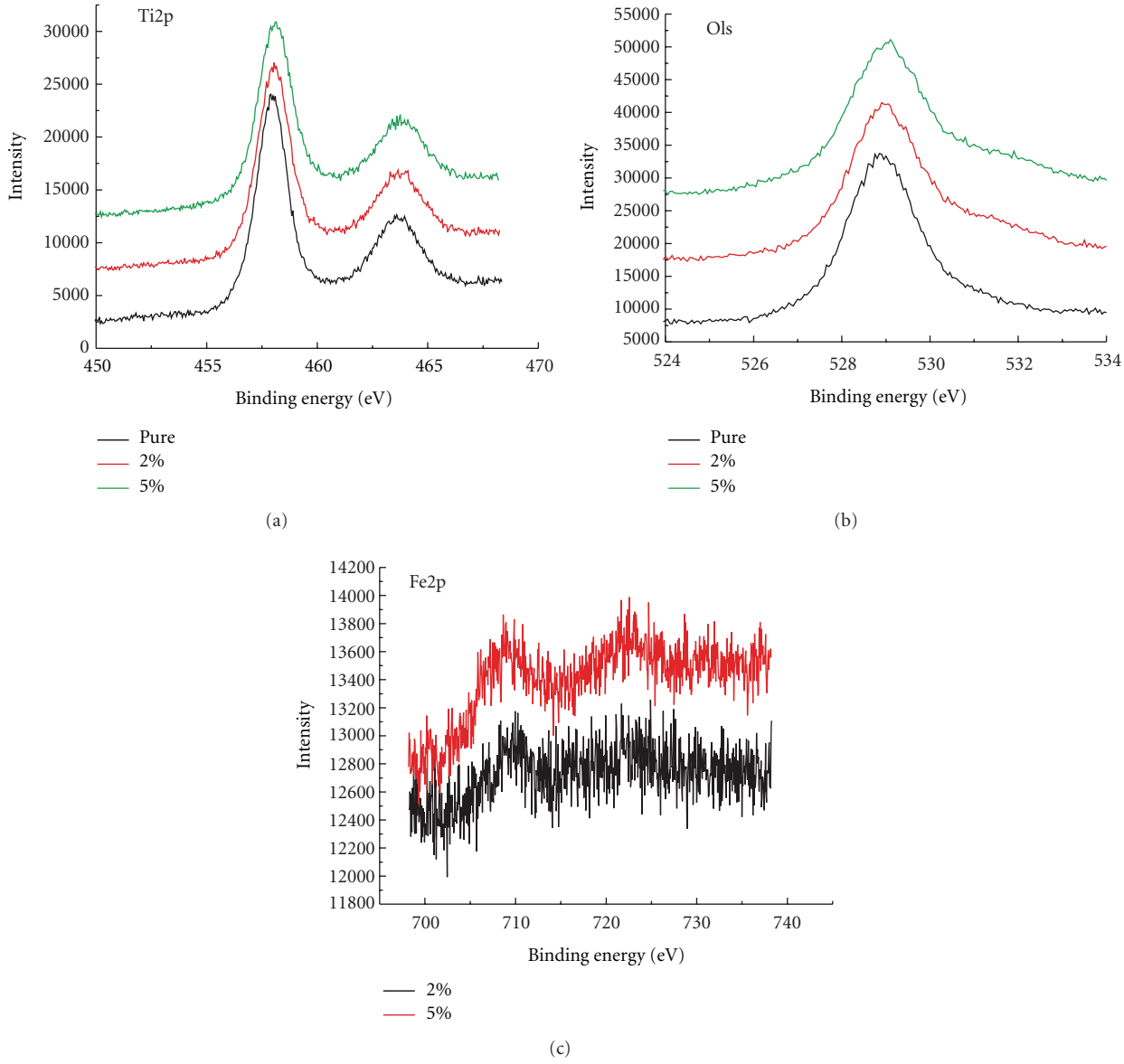

Figure 3: The O1s, Ti2p, and Fe2p core XPS spectra of 0.0, 2.0, and 5.0% Fe-doped TiO_2 samples.

exchange-correction functional in describing excited states. The theoretical study indicates that oxygen vacancy can be easily introduced by Fe doping [44], so the electronic structure of reduced anatase was also investigated, which is shown Figure 6(b). The E_F shifts to CB because some Ti^{4+} ions are reduced as Ti^{3+}, and some energy levels related to oxygen defects appeared at the CB bottom (labeled as the arrow). The E_g is narrowed by downshifting the CB bottom ca. 0.2 eV, which is in agreement with other reports [45, 46]. For the supercell containing a Fe^{3+} ion, the Fe3d orbitals split into two bands (Figure 6(c)). The upper hybrid band with CB is mainly composed of d_{z2} and d_{x2-y2} (A2g), and the intergap band consists of d_{zx}, d_{xy}, and d_{zy} (T2g), ~0.5 eV above the VB top. The T2g-A2g distance is about 1.8 eV. Because E_F is in the middle of T2g band, the electrons mainly occupy T2g band, and the A2g band is empty. Therefore, T2g → A2g transition is possible, which is the d-d transition in the UV-Vis DRS spectra. In addition, the hybrid A2g band partly contributes to the DRS red shift. When an oxygen vacancy is introduced in the Fe-doped anatase (Figure 6(d)), the Fe3d orbitals are still composed of two subbands, one midgap band (T2g) and one hybrid band (A2g). However, the T2g band is ca. 1.2 eV above the VB top, and the T2g-A2g distance is reduced to 0.9 eV due to the weakening of the crystal field effect. The E_F is almost at the top of A2g band because the electrons in oxygen vacancy are shared by the two adjacent Fe ions, which may be the reason that no Ti^{3+} ions are detected from XPS spectra. Consequently, DFT computation gives a clear result that the Fe doping will induce localized bandgap states, namely, T2g band.

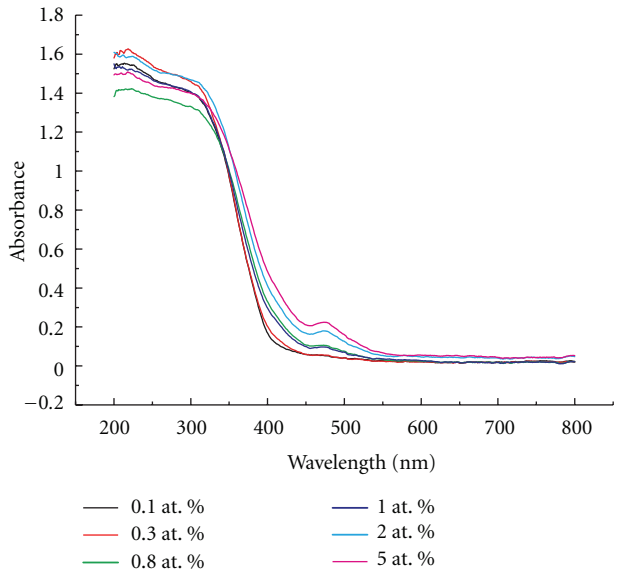

Figure 4: The DRS UV-Vis spectra of Fe-doped TiO_2 nanoparticles.

3.3. Photocatalytic Performance Evaluation. Figure 7(a) shows the dependence of $\ln(C_0/C)$ on time of the Fe-doped TiO_2 samples photodecomposing MO aqueous solution. Figure 7(b) shows the UV-Vis absorption spectra of MO aqueous solution for different periods of UV light illumination time for 0.3 at. % doped TiO_2. The blank experiment shows that the MO cannot be degraded in the absence of either TiO_2 or UV light. The Fe doping obviously influences the photocatalytic activity under UV light illumination. The 0.3 at. % Fe-doped sample has the best activity, better than the photocatalytic activity of P25. An optimal Fe concentration for the Fe-doped TiO_2 to present the best photocatalytic activity was observed, which is not a surprise because this has been seen for many times. Although it is stated that the Fe ions mainly form trapping centers for holes and electrons for low doping level, while they will become recombination centers for high doping [47], the mechanism of this trapping to recombination transformation is still unclear and in debate.

As shown by DFT calculation, the Fe3d T2g band is half-filled, and thus, The Fe^{3+} ions not only can trap electrons but also can trap holes. From the viewpoint of crystal field theory [17, 19, 20], the Fe ions after trapping a hole (Fe^{4+}) or an electron (Fe^{2+}) are unstable, and can favorably go back to Fe^{3+} ions by releasing an electron and hole. In general, there are some ways to resume Fe^{3+} ions. Firstly, the trapped electrons in Fe ions can migrate to TiO_2 surface via multitrapping. However, this multitrapping needs to overcome the potential barrier between Fe3d T2g band and TiO_2 CB, and the DFT calculation shows that this barrier is too high for the multitrapping to take place. In addition, the trapped electrons can migrate to the adjacent Fe site via hopping. Obviously, the hopping is difficult because Fe3d T2g states are almost localized according to the DFT calculation. Finally, the only possible pathway for Fe^{4+} and Fe^{2+} ions to regenerate Fe^{3+} ions is to recombine with the holes in VB, which are also supported by the PL

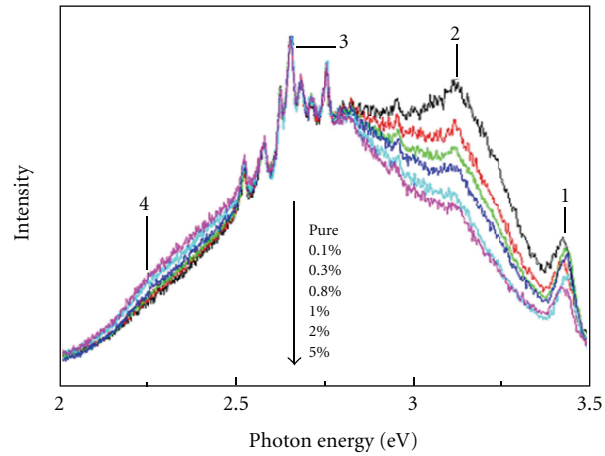

Figure 5: The PL spectra Fe-doped TiO_2 nano particles.

spectra. Therefore, the bulk-doped Fe ions mainly form the recombination centers of electrons and holes; more Fe ions entering TiO_2 bulk cannot contribute to the photocatalysis.

Compared with the Fe^{3+} ions in bulk, the Fe^{3+} ions on surface have different coordination environment. They can directly combine with the oxygen molecule (Fe–O_2) or the hydroxyl groups (Fe–OH), so the electrons or holes trapped on surface Fe^{3+} ions are possible to transfer to O_2 and –OH, resulting in the formation of O^{2-} and •OH, which has also been reported by others. Therefore, the Fe ions on surface can form intermediate pathways for the interfacial transfer. Because the surface recombination of the trapped electrons and holes is generally much slower than the interfacial transfer [48], the presence of Fe^{3+} ions on surface is useful to improve photocatalytic speed.

For the present experiment, the Fe^{3+} ions are not uniformly distributed in TiO_2 nanoparticles. In the case of low-level doping, they are mainly on TiO_2 surface. According to the above discussion, it can be known that the Fe ions mainly form the pathway for the electron-hole transfer for low doping concentration, so the photocatalytic activity will increase with the increase of doping concentration. For high-level doping, many Fe^{3+} ions can be doped in bulk beside those on the surface, so the recombination through the bulk Fe^{3+} ions cannot be neglected. Therefore, the photocatalytic activity firstly increases and then decreases with the increase of doped Fe content. It is widely accepted that the doped Fe^{3+} ions will change from the trapping centers to recombination centers as the doped concentration increases, how this change takes place is still not clear. It is claimed that the tunnel recombination through Fe ions is the reason of this trapping to recombination changing. We give new explanation of the trapping to recombination changing with the increase of Fe concentration, which is related to surface doping and bulk doping, as illustrated above.

4. Conclusion

The Fe-doped TiO_2 nanoparticles are prepared using hydrothermal method. It is confirmed that Fe^{3+} ions are

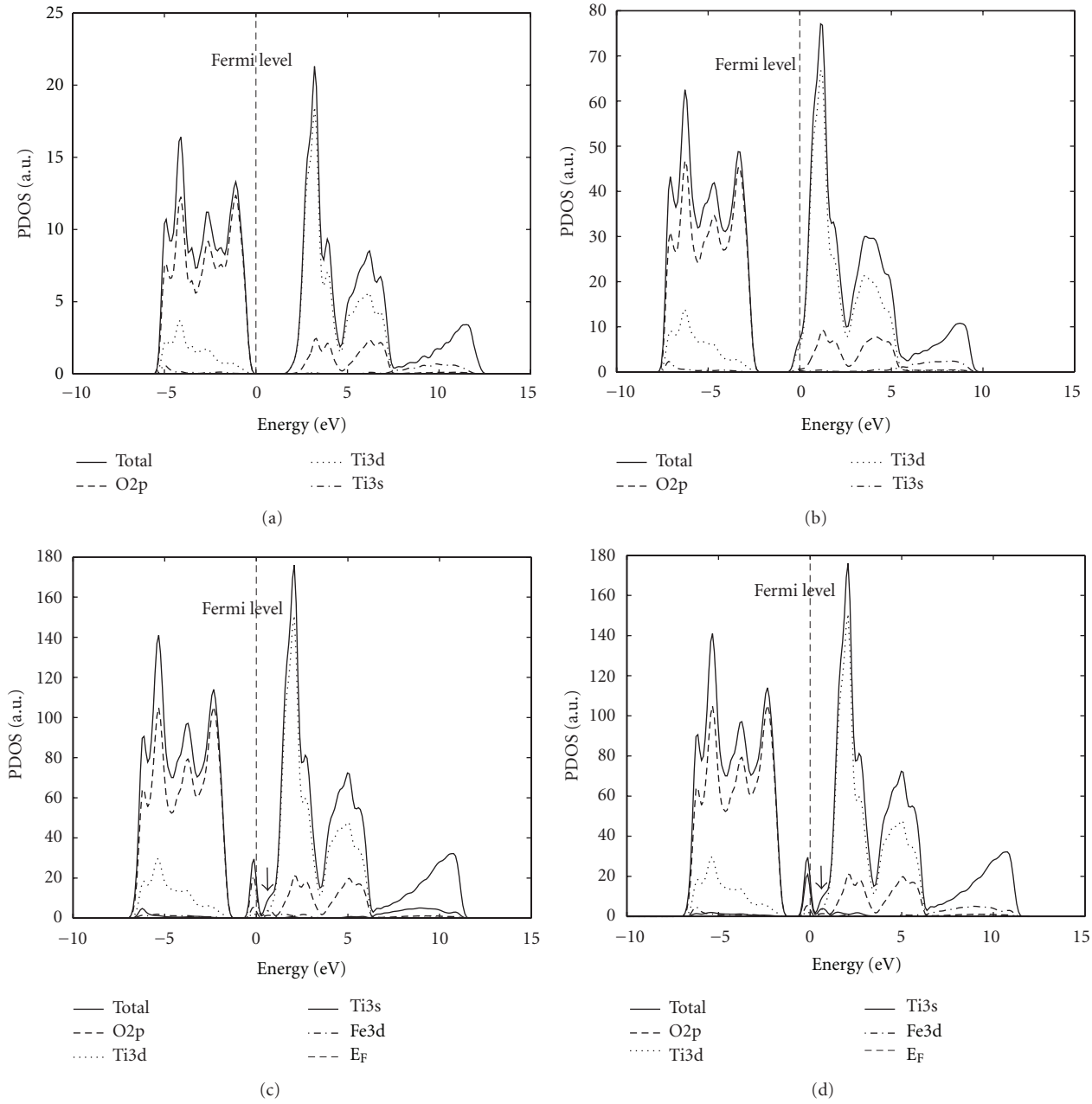

Figure 6: The PDOS of pure TiO_2 (a), 48 atom supercell containing one oxygen defect (b), 48 atom supercell containing a Fe ion (c), and 108 atom supercell containing two adjacent Fe ions and oxygen defect (d).

mainly doped on TiO_2 surface for low doping concentration, and some Fe ions will enter TiO_2 bulk for high doping concentration. The experiments and DFT calculation show that the Fe^{3+} ions in TiO_2 bulk are localized, so they mainly form the recombination centers. The Fe^{3+} ions on surface can form bridges for the transfer of electrons and holes, so surface doping is beneficial to the photocatalysis. It is observed that the photocatalytic activity of as-prepared Fe-doped TiO_2 firstly increases and then decreases with the increase of doping concentration, which is due to the trapping to recombination changing of doped Fe^{3+} ions. It is confirmed that this changing is related to the increase of bulk doping as the doped concentration increases.

Acknowledgments

This research was partly financially supported by NFSC (no. 50702041), and thanks to the supporting of Wuhan Young Scientists Chenguang Plan (no. 20091j0080) and the National Basic Research Program of China (2009CB939704). This research was also supported by Japan Society for the Promotion of Science (JSPS) for a postdoctoral fellowship

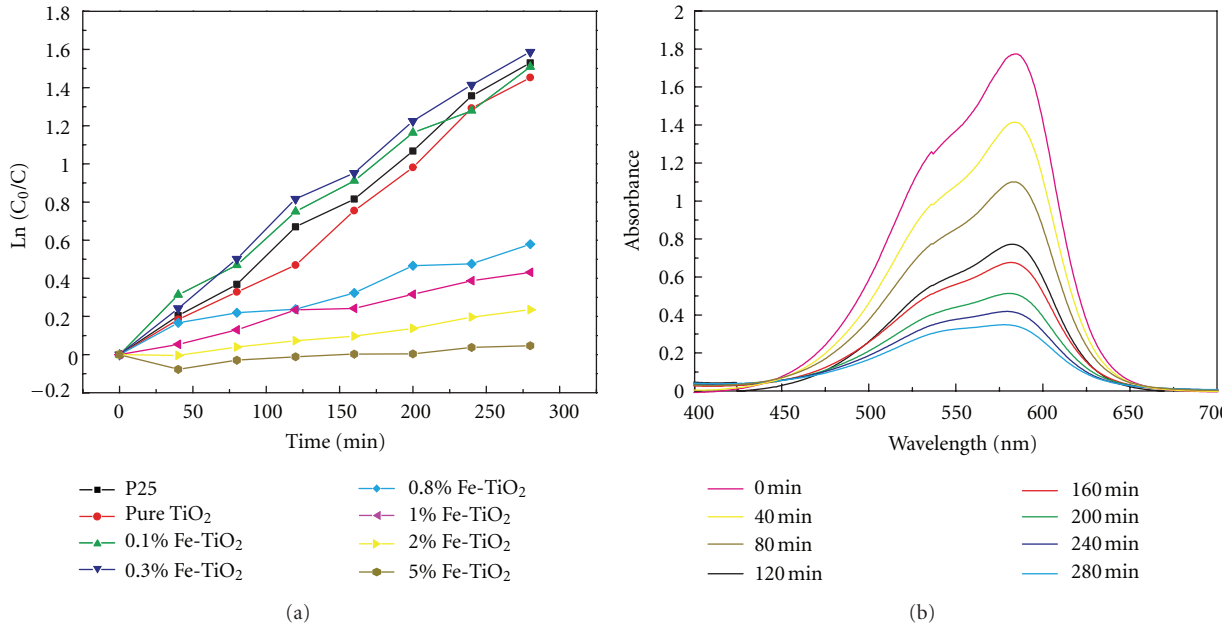

FIGURE 7: (a) The dependence of $\ln(C_0/C)$ on the UV illumination time of Fe-doped TiO_2 and (b) the absorption spectra of MO aqueous solution at different time span of UV light illumination.

for foreign researchers, and a scientific research (B) from the Ministry of Education, Culture, Sports, Science and Technology (MEXT), Japan.

References

[1] A. Fujishima and K. Honda, "Electrochemical photolysis of water at a semiconductor electrode," *Nature*, vol. 238, no. 5358, pp. 37–38, 1972.

[2] U. I. Gaya and A. H. Abdullah, "Heterogeneousphotocatalyticdegradation of organic contaminants over titanium dioxide: a review of fundamentals, progress and problems," *Journal of Photochemistry and Photobiology C*, vol. 9, no. 1, pp. 1–12, 2008.

[3] J. R. Jennings, A. Ghicov, L. M. Peter, P. Schmuki, and A. B. Walker, "Dye-sensitized solar cells based on oriented TiO_2 nanotube arrays: transport, trapping, and transfer of electrons," *Journal of the American Chemical Society*, vol. 130, no. 40, pp. 13364–13372, 2008.

[4] D. Kuang, J. Brillet, P. Chen et al., "Application of highly ordered TiO_2 nanotube arrays in flexible dye-sensitized solar cells," *ACS Nano*, vol. 2, no. 6, pp. 1113–1116, 2008.

[5] M. R. Hoffmann, S. T. Martin, W. Choi, and D. W. Bahnemann, "Environmental applications of semiconductor photocatalysis," *Chemical Reviews*, vol. 95, no. 1, pp. 69–96, 1995.

[6] C. Kormann, D. W. Bahnemann, and M. R. Hoffmann, "Photolysis of chloroform and other organic molecules in aqueous TiO_2 suspensions," *Environmental Science and Technology*, vol. 25, no. 3, pp. 494–500, 1991.

[7] S. Sakthivel, M. Janczarek, and H. Kisch, "Visible light activity and photoelectrochemical properties of nitrogen-doped TiO_2," *Journal of Physical Chemistry B*, vol. 108, no. 50, pp. 19384–19387, 2004.

[8] D. Chen, Z. Jiang, J. Geng, Q. Wang, and D. Yang, "Carbon and nitrogen co-doped TiO_2 with enhanced visible-light photocatalytic activity," *Industrial and Engineering Chemistry Research*, vol. 46, no. 9, pp. 2741–2746, 2007.

[9] S. In, A. Orlov, R. Berg et al., "Effective visible light-activated B-doped and B,N-codoped TiO_2 photocatalysts," *Journal of the American Chemical Society*, vol. 129, no. 45, pp. 13790–13791, 2007.

[10] S. Tojo, T. Tachikawa, M. Fujitsuka, and T. Majima, "Iodine-doped TiO_2 photocatalysts: Correlation between band structure and mechanism," *Journal of Physical Chemistry C*, vol. 112, no. 38, pp. 14948–14954, 2008.

[11] H. Ozaki, S. Iwamoto, and M. Inoue, "Effects of amount of Si addition and annealing treatment on the photocatalytic activities of N- and Si-codoped titanias under visible-light irradiation," *Industrial and Engineering Chemistry Research*, vol. 47, no. 7, pp. 2287–2293, 2008.

[12] N. Lu, X. Quan, J. Li, S. Chen, H. Yu, and G. Chen, "Fabrication of boron-doped TiO_2 nanotube array electrode and investigation of its photoelectrochemical capability," *Journal of Physical Chemistry C*, vol. 111, no. 32, pp. 11836–11842, 2007.

[13] T. Hirakawa and Y. Nosaka, "Selective production of superoxide ions and hydrogen peroxide over nitrogen- and sulfur-doped TiO_2 photocatalysts with visible light in aqueous suspension systems," *Journal of Physical Chemistry C*, vol. 112, no. 40, pp. 15818–15823, 2008.

[14] R. Asahi, T. Morikawa, T. Ohwaki, K. Aoki, and Y. Taga, "Visible-light photocatalysis in nitrogen-doped titanium oxides," *Science*, vol. 293, no. 5528, pp. 269–271, 2001.

[15] P. E. Lippens, A. V. Chadwick, A. Weibel, R. Bouchet, and P. Knauth, "Structure and chemical bonding in Zr-doped anatase TiO_2 nanocrystals," *Journal of Physical Chemistry C*, vol. 112, no. 1, pp. 43–47, 2008.

[16] J. Yu and H. Yu, "Preparation, characterization and photocatalytic activity of in situ Fe-doped TiO_2 thin films," *Thin Solid Film*, vol. 496, no. 2, pp. 273–280, 2006.

[17] M. Zhou, J. Yu, and B. Cheng, "Effects of Fe-doping on the photocatalytic activity of mesoporous TiO_2 powders prepared by an ultrasonic method," *Journal of Hazardous Materials*, vol. 137, no. 3, pp. 1838–1847, 2006.

[18] A. Mattsson, M. Leideborg, K. Larsson, G. Westing, and L. Österlund, "Adsorption and solar light decomposition of acetone on anatase TiO_2 and niobium doped TiO_2 thin films," *Journal of Physical Chemistry B*, vol. 110, no. 3, pp. 1210–1220, 2006.

[19] J. Yu, Q. Xiang, and M. Zhou, "Preparation, characterization and visible-light-driven photocatalytic activity of Fe-doped titania nanorods and first-principles study for electronic structures," *Applied Catalysis B*, vol. 90, no. 3-4, pp. 595–602, 2009.

[20] W. Choi, A. Termin, and M. R. Hoffmann, "The role of metal ion dopants in quantum-sized TiO_2: correlation between photoreactivity and charge carrier recombination dynamics," *Journal of Physical Chemistry*, vol. 98, no. 51, pp. 13669–13679, 1994.

[21] J. Zhu, F. Chen, J. Zhang, H. Chen, and M. Anpo, "Fe^{3+}-TiO_2 photocatalysts prepared by combining sol-gel method with hydrothermal treatment and their characterization," *Journal of Photochemistry and Photobiology A*, vol. 180, no. 1-2, pp. 196–204, 2006.

[22] T. Tong, J. Zhang, B. Tian, F. Chen, and D. He, "Preparation of Fe^{3+}-doped TiO_2 catalysts by controlled hydrolysis of titanium alkoxide and study on their photocatalytic activity for methyl orange degradation," *Journal of Hazardous Materials*, vol. 155, no. 3, pp. 572–579, 2008.

[23] J. Wang, Z. Liu, and R. Cai, "A new role for Fe^{3+} in TiO_2 hydrosol: accelerated photodegradation of dyes under visible light," *Environmental Science and Technology*, vol. 42, no. 15, pp. 5759–5764, 2008.

[24] H. Yu, H. Irie, and K. Hashimoto, "Conduction band energy level control of titanium dioxide: toward an efficient visible-light-sensitive photocatalyst," *Journal of the American Chemical Society*, vol. 132, no. 20, pp. 6898–6899, 2010.

[25] H. Irie, S. Miura, K. Kamiya, and K. Hashimoto, "Efficient visible light-sensitive photocatalysts: grafting Cu(II) ions onto TiO_2 and WO_3 photocatalysts," *Chemical Physics Letters*, vol. 457, no. 1–3, pp. 202–205, 2008.

[26] Z. Zhang, C. C. Wang, R. Zakaria, and J. Y. Ying, "Role of particle size in nanocrystalline TiO_2-based photocatalysts," *Journal of Physical Chemistry B*, vol. 102, no. 52, pp. 10871–10878, 1998.

[27] http://www.quantum-espresso.org/

[28] S. Ardizzone, C. L. Bianchi, G. Cappelletti, S. Gialanella, C. Pirola, and V. Ragaini, "Tailored anatase/brookite nanocrystalline TiO_2. The optimal particle features for liquidand gas-phase photocatalytic reactions," *Journal of Physical Chemistry C*, vol. 111, no. 35, pp. 13222–13231, 2007.

[29] A. Testino, I. R. Bellobono, V. Buscaglia et al., "Optimizing the photocatalytic properties of hydrothermal TiO_2 by the control of phase composition and particle morphology. A systematic approach," *Journal of the American Chemical Society*, vol. 129, no. 12, pp. 3564–3575, 2007.

[30] J. G. Yu, M. H. Zhou, B. Cheng, and X. J. Zhao, "Preparation, characterization and photocatalytic activity of in situ N,S-codoped TiO_2 powders," *Journal of Molecular Catalysis A*, vol. 246, no. 1-2, pp. 176–184, 2006.

[31] B. Liu, X. Zhao, Q. Zhao, C. Li, and X. He, "The effect of O_2 partial pressure on the structure and photocatalytic property of TiO_2 films prepared by sputtering," *Materials Chemistry and Physics*, vol. 90, no. 1, pp. 207–212, 2005.

[32] Y. Lv, Y. Ding, J. Zhou, W. Xiao, and Y. Feng, "Preparation, characterization, and photocatalytic activity of N, S-codoped TiO_2 nanoparticles," *Journal of the American Ceramic Society*, vol. 92, no. 4, pp. 938–941, 2009.

[33] B. Liu, L. Wen, and X. Zhao, "The surface change of TiO_2 film induced by UV illumination and the effects on UV-vis transmission spectra," *Applied Surface Science*, vol. 255, no. 5, pp. 2752–2758, 2008.

[34] H. Choi, M. G. Antoniou, M. Pelaez, A. A. De La Cruz, J. A. Shoemaker, and D. D. Dionysiou, "Mesoporous nitrogen-doped TiO_2 for the photocatalytic destruction of the cyanobacterial toxin microcystin-LR under visible light irradiation," *Environmental Science and Technology*, vol. 41, no. 21, pp. 7530–7535, 2007.

[35] Z. Ambrus, N. Balázs, T. Alapi et al., "Synthesis, structure and photocatalytic properties of Fe(III)-doped TiO_2 prepared from TiCl3," *Applied Catalysis B: Environmental*, vol. 81, no. 1-2, pp. 27–37, 2008.

[36] B. Liu, X. Wang, G. Cai, L. Wen, Y. Song, and X. Zhao, "Low temperature fabrication of V-doped TiO_2 nanoparticles, structure and photocatalytic studies," *Journal of Hazardous Materials*, vol. 169, no. 1–3, pp. 1112–1118, 2009.

[37] K. S. W. Sing, D. H. Everett, R. A. W. Haul et al., "Reporting physisorption data for gas/solid systems with special reference to the determination of surface area and porosity," *Pure and Applied Chemistry*, vol. 57, no. 4, pp. 603–619, 1984.

[38] B. Liu, L. Wen, and X. Zhao, "The photoluminescence spectroscopic study of anatase TiO_2 prepared by magnetron sputtering," *Materials Chemistry and Physics*, vol. 106, no. 2-3, pp. 350–353, 2007.

[39] B. Liu, X. Zhao, and L. Wen, "The structural and photoluminescence studies related to the surface of the TiO_2 sol prepared by wet chemical method," *Materials Science and Engineering B*, vol. 134, no. 1, pp. 27–31, 206.

[40] Y. Cong, J. Zhang, F. Chen, M. Anpo, and D. He, "Preparation, photocatalytic activity, and mechanism of nano-TiO_2 Co-doped with nitrogen and iron (III)," *Journal of Physical Chemistry C*, vol. 111, no. 28, pp. 10618–10623, 2007.

[41] H. Tang, K. Prasad, R. Sanjinès, P. E. Schmid, and F. Lévy, "Electrical and optical properties of TiO_2 anatase thin films," *Journal of Applied Physics*, vol. 75, no. 4, pp. 2042–2047, 1994.

[42] T. L. Villarreal, R. Gómez, M. González, and P. Salvador, "A kinetic model for distinguishing between direct and indirect interfacial hole transfer in the heterogeneous photooxidation of dissolved organics on TiO_2 nanoparticle suspensions," *Journal of Physical Chemistry B*, vol. 108, no. 52, pp. 20278–20290, 2004.

[43] K. Yang, Y. Dai, and B. Huang, "First-principles calculations for geometrical structures and electronic properties of Si-doped TiO_2," *Chemical Physics Letters*, vol. 456, no. 1–3, pp. 71–75, 2008.

[44] A. Roldán, M. Boronat, A. Corma, and F. Illas, "Theoretical confirmation of the enhanced facility to increase oxygen vacancy concentration in TiO_2 by iron doping," *Journal of Physical Chemistry C*, vol. 114, no. 14, pp. 6511–6517, 2010.

[45] I. Justicia, P. Ordejon, G. Canto et al., "Designed self-doped titanium oxide thin films for efficient visible-light photocatalysis," *Advanced Materials*, vol. 14, no. 19, pp. 1399–1402, 2002.

[46] F. Zuo, L. Wang, T. Wu, Z. Zhang, D. Borchardt, and P. Feng, "Self-doped Ti^{3+} enhanced photocatalyst for hydrogen production under visible light," *Journal of the American Chemical Society*, vol. 132, no. 34, pp. 11856–11857, 2010.

[47] M. Grätzel, *Heterogeneous Photochemical Electron Transfer Reactions*, CRC Press, Boca Raton, Fla, USA, 1987.

[48] B. Liu, K. Nakata, X. Zhao, T. Ochiai, T. Murakami, and A. Fujishima, "Theoretical kinetic analysis of heterogeneous photocatalysis: the effects of surface trapping and bulk recombination through defects," *The Journal of Physics and Chemistry*, vol. 115, no. 32, pp. 16037–16042, 2011.